JOURNAL OF GEOPHYSICAL RESEARCH, VOL. 100, NO. D7, PAGES 14,243–14,255, JULY 20, 1995

Low-wavenumber spectral characteristics of velocity and temperature in the atmospheric surface layer

Gabriel G. Katul
School of the Environment, Duke University, Durham, North Carolina

Chia R. Chu
Department of Civil Engineering, National Central University, Taiwan, R.O.C.

Marc B. Parlange, John D. Albertson, and Teresa A. Ortenburger
Hydrologic Science, University of California, Davis

Abstract. The structure of atmospheric surface layer turbulence at low wavenumbers was analyzed using 56 Hz triaxial velocity and temperature measurements above a uniform dry lake bed. A key feature of this experiment was the small roughness length of the surface that resulted in a small roughness Reynolds number. Under near-neutral atmospheric stability conditions, a -1 power law was observed in both measured velocity and temperature spectra which is consistent with previously proposed dimensional analysis for rough and smooth turbulent boundary layer flows. The wavenumber at which the -1 power law terminates and the -5/3 power law commences was derived as a function of the Kolmogorov and von Karman constants. Good agreement between the predicted and the measured transition wavenumber from -1 to -5/3 was noted for fully rough-flow conditions. However, this was not the case for other roughness conditions. The similarity theory constants for the neutral case were determined and they compared favorably with other laboratory and field studies. For unstable atmospheric conditions, directional dimensional analysis was used to predict the slopes of the power spectra of temperature and velocity. It was demonstrated that for moderately unstable conditions, the temperature and vertical velocity power spectra exhibited a -1 power law, but the longitudinal velocity exhibited a -2 power law. The agreement between predicted and measured power laws was within experimental errors. Some differences between the constants determined from this experiment and other experiments are also discussed.

1. Introduction

The exchange of heat and momentum between the Earth surface and the atmosphere is controlled by eddy motion in the atmospheric surface layer (ASL). Within the surface layer, the spectrum of eddy sizes extends over a wide range and can be divided into three broad categories: (1) production scales, in which energy is extracted from the mean flow and injected into turbulence; (2) inertial subrange scales, in which energy cascades down to smaller scales through vortex stretching; and (3) viscous dissipation scales, in which energy is dissipated by the action of fluid viscosity. Among the three categories, the production scales are most responsible for the heat and momentum exchanges between the atmosphere and the land surface.

Paper number 94JD02616.
0148-0227/95/94JD-02616 $05.00

Much attention has been devoted to the structure of the inertial subrange, and numerous experiments in the ASL and laboratories have investigated its spectral and spatial structure [*Monin and Yaglom*, 1975, Chap. 8] as predicted by *Kolmogorov's* [1941] scaling theory. However, no complete theory has yet been developed for the production scales in the atmospheric surface layer.

The possibility that production scales in wall-bounded shear flow possess a universal spectral behavior was first proposed by *Tchen* [1953]. He found that the production range of the longitudinal velocity spectrum is proportional to K_1^{-1}, where K_1 is the one-dimensional wavenumber in the longitudinal direction. *Tchen*'s prediction was based on order of magnitude argument for the velocity fluctuating part of the Navier-Stokes equation

$$\frac{\partial u'_i}{\partial t}+\frac{\partial}{\partial x_j}(u'_i\langle U_i\rangle) = \nu\frac{\partial^2 u'_i}{\partial x_j\partial x_j}-\frac{\partial}{\partial x_j}(u'_j\langle U_i\rangle)- \frac{\partial}{\partial x_j}(u'_iu'_j-\langle u'_iu'_j\rangle+\frac{p'}{\rho}\delta_{ij}) \quad (1)$$

where t is time, x_i are the space coordinates (x_1 is the longitudinal wind direction, x_2 is the lateral direction, and x_3 is the vertical direction), u'_i are the velocity fluctuations, p' is the pressure fluctuation, ρ is the density and ν is the kinematic viscosity. Primes indicate fluctuations around time averages and $<.>$ is the time-averaging operator. *Tchen* [1953] noted that the interaction between the large-scale eddies and the mean flow is controlled by the terms involving $u'_i<U_j>$ and $u'_j<U_i>$. He concluded that the spectrum of u'_1 is proportional to K_1^{-1} when the vorticity of the mean flow is large and interacting with the turbulent motion. Later, *Klebanoff* [1954] conducted an experiment to study flat plate boundary layer without pressure gradient. His results support *Tchen*'s prediction for the u'_1 spectrum (E_1) at low wavenumbers, especially for $z/\delta \sim 0.05$, where δ is the boundary layer height and z is the measurement height along the x_3 direction (see also *Hinze*, [1959], p. 501). It is noted that in *Klebanoff*'s experiment, E_1 did not exhibit a -1 power law for $z/\delta = 0.0011$ and $z/\delta = 0.8$. This suggests that the -1 power law occurs in the proximity of the wall boundary, yet far enough away so that viscous effect has negligible influence on the large scales. *Hinze* [1959] proposed that at $z/\delta = 0.05$, strong production of turbulent energy takes place. As z/δ decreases, the contribution of larger eddies to the turbulent energy reduces at the low wavenumber end but increases at the high wavenumber end of the energy spectrum.

Experiment for fully developed turbulent air flow in pipe by *Perry and Abell* [1975] focused on the scaling properties of E_1 in the overlap region between the "inner flow" and the "outer flow." The well-known logarithmic mean velocity profile originally derived by *von Karman* [1930] and *Millikan* [1939] exists in this region. *Perry and Abell* [1975] found that E_1 is proportional to K_1^{-1} for low wavenumbers; however, not for $E_3(K_1)$. This result was independently confirmed by *Korotkov* [1976] using channel flow data. Later, *Perry and Chong* [1982] proposed dimensional analysis argument consistent with the attached-eddy hypothesis of *Townsend* [1976, pp.150-156] to explain the behavior of E_1 at small wavenumbers (see also *Perry and Li* [1990]). The attached eddy hypothesis of *Townsend* [1976] assumes that the main eddies are persistent, organized and attached to the wall boundary. The analysis of *Perry and Chong* [1982] was successful in linking the logarithmic profile of the mean velocity and the dependence of E_1 on K_1^{-1}. However, they failed to reproduce the *Kolmogorov* [1941] scaling for the inertial subrange. Later, analysis by *Perry et al.* [1986] assumed that large-scale coherent eddies are surrounded by a fluid which contains fine-scale detached eddies. The motion of these detached eddies is assumed to be locally isotropic and contributing little to the turbulent stresses. These detached eddies are simply the remainder of what were once attached eddies that have been stretched, distorted and convected away from the wall boundary by other attached eddies (see *Perry et al.* [1991, 1994] for a detailed review). Therefore the attached eddies are independent of viscosity and scale with mean-flow variables, while the detached eddies scale with the mean turbulent energy dissipation rate $<\epsilon>$ and follow the *Kolmogorov* [1941] scaling.

Based on the analysis of *Perry et al.* [1986, 1987], *Erm and Joubert* [1991] reconsidered the structure of low Reynolds number turbulent boundary layer over a smooth flat surface with zero pressure gradients. They noted that a -1 power law exists in the u'_1 and u'_3 power spectra for $z/\delta = 0.1$, analogous to the spectra of *Perry et al.* [1986] at large Reynolds number. However, the -1 power law scaling was not apparent in the velocity spectra for $z/\delta > 0.35$. Although *Erm and Joubert*'s [1991] analysis was restricted to low Reynolds number turbulence, the -1 power law scaling appeared insensitive to the magnitude of the Reynolds number provided the flow is turbulent (the Reynolds number was of the order of 1000, defined using the momentum displacement height).

The -1 power law behavior was also noted in the temperature (T) spectrum (E_T) at low wavenumbers from a large eddy simulation (LES) performed by *Lesieur and Rogallo* [1989]. The LES described a flow domain of 128^3 collocation points for decaying isotropic turbulence convecting a passive temperature admixture. Later LES runs by *Metais* [1991] and *Metais and Lesieur* [1992] confirmed that the temperature spectrum tends to follow, in the energetic scales, a K_1^{-1} relationship followed by a $K_1^{-5/3}$. The occurrence of the -1 power law at small wavenumbers was attributed to the straining of the temperature fluctuations by the velocity gradients [*Lesieur and Rogallo*, 1989]. The probability density functions (PDFs) computed from the LES of *Metais* [1991] and *Metais and Lesieur* [1992] demonstrate that the tails of the u'_1 PDF are Gaussian (i.e., $\sim \exp(-X^2)$) and that the tails of the T', $\partial u'_1/\partial x_3$ and $\partial u'_3/\partial x_1$ PDFs are exponential (i.e., $\sim \exp(-X)$). The exponential tails observed in the longitudinal velocity gradient and the temperature PDFs appear to support the working hypothesis that the temperature fluctuations are strained by the velocity field. However, the LES simulations of *Lesieur and Rogallo* [1989] and *Metais* [1991] did not exhibit a -1 power law for the E_1 spectrum. The LES predictions for E_1 were proportional to $K_1^{-5/3}$. Further LES runs by *Metais and Lesieur* [1992] under stable buoyant conditions produced a temperature spectrum that did not exhibit a -1 power law and appeared to follow closely the scaling of the velocity spectrum.

Raupach et al. [1991] and *Antonia and Raupach* [1993] discussed the existence of a -1 power law scaling for E_1 and E_3 in rough wall boundary layers but argued against its existence in the ASL based on the experiment by *Kaimal et al.* [1972]. They attributed the general absence of the K_1^{-1} scaling to the buoyancy effects that are present in the ASL but absent in the outer region of many laboratory boundary layers. Extensive atmospheric spectral data have been measured in several major field experiments, one of the largest being in Kansas [1968]. Instrumentation for the Kansas experiment included three triaxial sonic anemometers mounted at 5.66, 11.3 and 22.6 m [*Kaimal et al.*, 1972]. Their experiment confirmed the existence of a -5/3 law as predicted by *Kolmogorov's* [1941] theory for all velocity components. However, the occurrence of a -1 power law scaling at the low-frequency end was not reported. These questions regarding the existence of a -1 power law at the low wavenumber end of the velocity and temperature spectra have motivated this study. In this study we examine the possibility that a -1 power law exists in the ASL at low wavenumber with possible deviation due to buoyancy. An experiment involving triaxial sonic anemometer velocity and temperature measurements was carried out over a uniform dry lake bed (28 km x 14 km) under different atmospheric stability conditions. The site is characterized by a desert climate with surface temperatures up to 65°C during the day-time. The lake bed consists of sandy soil with an average momentum roughness length of $z_o = 0.13$ mm. Therefore in many cases the flow was not fully rough. This adds to the uniqueness of the experiment since smooth-walled boundary layer flows in the natural environment have not been rigorously investigated, yet they play a key role in many climate and mesoscale models, especially models related to the study of desert [*Peixoto and Oort*, 1992].

The neutral stability case is considered first to investigate the mechanism responsible for the turbulent energy production at low wavenumbers; this allows comparison with previous laboratory and numerical studies. Then we consider the spectrum at low wavenumbers and the transition to the inertial subrange for unstable atmospheric conditions. We also investigate the applicability of dimensional arguments proposed by *Betchov and Yaglom* [1971] and *Zilitinkevich* [1971, 1973] to the unstable

surface layer. These dimensional arguments were tested for the unstable ASL by *Kader and Yaglom* [1984, 1990, 1991] using an extensive data set collected at the Tsimlyansk field station of the Moscow Institute of Atmospheric Physics over a 7-year period. The formulation of these dimensional arguments is considered next.

2. Applications of Similarity Theory to Turbulent Fluctuations: General Considerations

Mean flow characteristics of ASL turbulence can be described by the following dimensional parameters:(1) the height above the ground z, (2) the friction velocity u_* $(=(\tau/\rho)^{1/2})$, (3) the buoyancy parameter β $(= g\gamma)$ and (4) the sensible H $(= c_p\rho\langle u_3' T'\rangle)$ and the latent L_vE $(= L_v \rho\langle u_3' q'\rangle)$ heat fluxes, where τ $(= -\rho\langle u_1'u_3'\rangle)$ is the surface shear stress, g is the gravitational acceleration, $\gamma = T^{-1}$ is the coefficient of thermal expansion (assuming air is an ideal gas), T is the mean absolute temperature, c_p and L_v are the heat capacity and the latent heat of vaporization, respectively, and q' and T' are the specific humidity and temperature fluctuations about mean values, respectively [e.g., *Monin and Obukhov*, 1954; *Monin and Yaglom*, 1971, Chap. 4; *Brutsaert*, 1982, Chaps. 3 and 4).

As discussed by *Monin and Yaglom* [1971, p. 457], the extension of similarity theory to the turbulent fluctuations requires, in a strict sense, that the joint probability distribution for the dimensionless fluctuations u'_1/u_*, u'_2/u_*, u'_3/u_*, T'/T_* be independent of the space-time origin and depend only on the normalized time lag and separation distance. Here, the time lags are normalized by L/u_* and the separation distances are normalized by the Obukhov length L

$$L = \frac{-\rho u_*^3}{kg\left[\left(\frac{H}{Tc_p}\right)+0.61E\right]} \tag{2}$$

where k(= 0.4) is the von Karman constant. This normalization requires that the separation distance be small enough so that Coriolis effects can be neglected, yet large enough so that viscous effects can also be neglected.

It is recognized that surface layer similarity theory, proposed by *Monin and Obukhov* [1954], is quite successful in describing mean flow characteristics [see *Brutsaert*, 1982; *Monin and Yaglom*, 1971]; however, only partial success was reported in describing the statistics of the fluctuating components [*Wyngaard*, 1992]. To improve some of the deficiencies of surface layer similarity theory, a more generalized dimensional scheme has been proposed by *Kader and Yaglom* [1990]. The study by *Kader and Yaglom* [1990] based on previous work by *Zilitinkevich* [1971, 1973], *Betchov and Yaglom* [1971], and *Kader and Yaglom* [1984] suggested that the ASL is comprised of three sublayers that each have a self-preserving turbulence statistical structure. These sublayers are (1) forced convective (or dynamic), (2) dynamic convective (or moderately unstable) and (3) free convective. Within the forced convective sublayer, the buoyancy parameter β can be excluded from the list of dimensional parameters. The free convective sublayer occurs when $z >> |L|$ and u_* can be omitted from the list of dimensional parameters. The dynamic convective sublayer occurs at moderate values of $\zeta = - z/L$ and all four dimensional parameters are important. The term "shear convection" was used by *Zilitinkevich* [1973] to describe this atmospheric sublayer. The distinction between these sublayers allows separate universal formulations of the power spectra and co-spectra (E_{ij}) of the velocity components (i = 1, 2, 3; j = 1, 2, 3) for wavenumbers (K_1) that are much smaller than the Kolmogorov dissipation scales and yet dynamically important.

The scaling behavior of the one-dimensional spectrum at production scales can be derived from dimensional arguments [*Tennekes and Lumley*, 1972, p. 264]. The velocity spectra E_1, E_2 and E_3 have units of $m^3 s^{-2}$ and scale with u_*, z and L, while the temperature spectrum E_T has units of $°C^2$ m and scales with T_* and z so that

$$\frac{E_i(K_1)}{u_*^2 z} = \chi_i(K_1 z, z/L)$$
$$\frac{E_T(K_1)}{T_*^2 z} = \chi_T(K_1 z, z/L) \tag{3}$$

where $\chi_i(.)$, $\chi_T(.)$ are dimensionless functions and $T_* = \langle u_3'T'\rangle/u_*$.

2.1. Forced Convective Sublayer ($|z/L|\to 0$)

For the case $z << |L|$ the stability parameter is no longer important (near-neutral conditions). Therefore $\chi_i(.)$ and $\chi_T(.)$ depend only on the product K_1z. In addition, if the large-scale fluctuations are on a scale much greater than z, then the spectra $E_i(K_1)$ and $E_T(K_1)$ will not be affected significantly by moderate changes in z (i = 1, 2, 3). Hence if K_1 z is small enough, we can eliminate z from (3) by requiring

$$\frac{E_i(K_1)}{u_*^2 z} = \frac{A_i}{K_1 z}$$
$$\frac{E_T(K_1)}{T_*^2 z} = \frac{B_T}{K_1 z} \tag{4}$$

which yields $E_i(K_1) = A_i u_*^2 K_1^{-1}$ and $E_T(K_1) = B_T T_*^2 K_1^{-1}$, where A_i and B_T are constants to be determined from experiments [*Kader and Yaglom*, 1984, 1991] and i = 1, 2, 3. Hence the height independence of the large-scale statistics for small z leads to a -1 power law for the temperature and velocity spectra. This may explain why in *Klebanoff*'s [1954] data, a -1 power law was measured at $z/\delta \sim 0.05$ but not for $z/\delta = 0.0011$ or $z/\delta = 0.8$. For $z/\delta = 0.0011$, viscous effects may have played a key role, while for $z/\delta = 0.8$, z was large and the statistics of the large-scale eddy motion cannot be independent of height. However, for $z/\delta = 0.05$, z was small enough so that small variations in z do not affect the statistics of the large scales (whose characteristic length scale is of the order δ and are responsible for much of the turbulent production).

2.2. Free Convective Sublayer ($|L|\to 0$)

For the case $z >> |L|$, u_* is no longer important and the velocity and temperature spectra can be derived using the

free-convective local scaling w_* ($=[gz\langle u_3' T'\rangle/T]^{1/3}$) and T_{**} ($=\langle u_3'T'\rangle/w_*$) [*Garratt*, 1992; *Stull*, 1988]. Hence the spectra of velocity and temperature scale are

$$\frac{E_i(K_1)}{w_*^2 z} = \chi_i^c(K_1 z)$$
$$\frac{E_T(K_1)}{T_{**}^2 z} = \chi_T^c(K_1 z) \qquad (5)$$

where $\chi_i^c(.)$ and $\chi_T^c(.)$ are dimensionless functions whose form for small wavenumbers is considered next. As shown by *Kader and Yaglom* [1984], using the height independence argument for the larger eddies at small z, the spectra for the velocity components and the temperature scale are

$$\frac{E_i(K_1)}{\left(\frac{g}{T}\langle u_3' T'\rangle z\right)^{2/3} z^{1/3}} = \frac{A_i^c}{(K_1 z)^{5/3}}$$
$$\frac{E_T(K_1)}{\left(\frac{g}{T}\right)^{-2/3}\langle u_3' T'\rangle^{4/3} z^{1/3}} = \frac{B_T^c}{(K_1 z)^{1/3}}. \qquad (6)$$

where A_i^c and B_T^c are constants to be determined from experiments and i = 1, 2, 3. Hence in dimensional form, the velocity and temperature spectra reduce to

$$E_i(K_1) = A_i^c\left(\frac{g}{T}\langle u_3' T'\rangle\right)^{2/3} K_1^{-5/3}$$
$$E_T(K_1) = B_T^c\left(\frac{g}{T}\right)^{-2/3}\langle u_3' T'\rangle^{4/3} K_1^{-1/3}. \qquad (7)$$

2.3. Directional Dimensional Analysis in the Dynamic Convective Sublayer

This section reviews the applicability of the concept of directional dimensional analysis (DDA), as proposed by *Kader and Yaglom* [1984, 1990] and *Zilitinkevich* [1973], to the turbulent fluctuations for the dynamic convective sublayer. In this sublayer, u_*, β, z and the heat fluxes are all important parameters. We restrict our discussion to the description of the velocity and temperature spectra at small wavenumbers. Within this sublayer the net energy exchange between the horizontal and the vertical motion is neglected (i.e., shear production and buoyant production are independent). The extent of the dynamic convective layer is $0.14 < |z/L| < 1.2$ [*Kader and Yaglom*, 1990]. The de-coupling between the horizontal and the vertical motions permits the application of DDA to the study of the spectra of velocity and temperature. DDA differs from the classical dimensional analysis by assuming that the horizontal and vertical motions have independent length scales, L_1 and L_3, respectively [see *Zilitinkevich*, 1973; *Panton*, 1984, pp. 181-228]. It is noted that a de-coupling of the vertical and horizontal energies is clearly unrealistic for a wide range of scales, especially the inertial subrange scales. The local isotropy that develops in the inertial subrange cannot be attained without energy exchanges between the horizontal and the vertical motion (through the pressure redistribution term). However, for the larger scales, this de-coupling assumption may be reasonable since buoyancy enters the dynamics of turbulence through the large-scale vertical motion and shear enters through the large-scale horizontal motion; these two production mechanisms are, to a first approximation, independent.

Using the two independent length scales for the horizontal and vertical dimensions (L_1 and L_3), the friction velocity u_* ($= -\langle u_1' u_3'\rangle^{1/2}$) has dimensions of $(L_1 L_3)^{1/2} t^{-1}$. Thus it is ill- suited as a scaling parameter for either the horizontal or the vertical motion (it involves both length scales). Hence we require two velocity scales, one for each direction of motion. The vertical motion may be scaled by w_* ($=[gz\langle u_3' T'\rangle/T]^{1/3}$) since it involves L_3 and is related to buoyancy; the horizontal motion may be scaled by u_{**} ($=u_*^2/w_*$) since it involves L_1 and is related to shear. Similarly, T_{**} ($=\langle u_3' T'\rangle/w_*$) defines a temperature scale and $l_* = (u_*/w_*)^2 z$ defines a horizontal length scale. Notice that all horizontal motion enters the turbulence dynamics through u_{**}, while the vertical motion enters through w_*.

As shown by *Kader and Yaglom* [1991], the general form of the one-dimensional temperature and velocity spectra can be defined as

$$\frac{E_i(K_1)}{u_{**}^2 l_*} = \chi_i^d(K_1 l_*) \qquad (i=1,2)$$
$$\frac{E_3(K_1)}{w_*^2 l_*} = \chi_3^d(K_1 l_*)$$
$$\frac{E_T(K_1)}{T_{**}^2 l_*} = \chi_T^d(K_1 l_*) \qquad (8)$$

where $\chi_i^d(.)$, $\chi_T^d(.)$ are similarity functions to be determined. Notice that l_* was used to normalize K_1 since K_1 represents wavenumber along the longitudinal direction (x_1). The form of $\chi_i^d(.)$, $\chi_T^d(.)$ can be inferred using the following arguments: (1) E_i (here i = 1, 2) is independent of the buoyancy parameter $\beta(= g T^{-1})$; and (2) E_3 and E_T are independent of shear and hence are independent of l_*. Notice the difference between these arguments and the height-independent argument previously used. Argument 1 implies that the buoyancy parameter β enters the turbulent kinetic energy equation only through the vertical motion. Also, if we note that u_* enters the vertical motion only through l_*, then argument 2 requires that E_3 and E_T be independent of u_*. For both arguments the large-scale eddy motion is dependent on height. Therefore the velocity and temperature spectra are given by the following dimensionless forms

$$\frac{E_1(K_1)}{u_{**}^2 l_*} = A_1^d(K_1 l_*)^{-2}$$
$$\frac{E_3(K_1)}{w_*^2 l_*} = A_3^d(K_1 l_*)^{-1}$$
$$\frac{E_T(K_1)}{T_{**}^2 l_*} = B_T^d(K_1 l_*)^{-1} \qquad (9)$$

where A_i^d and B_T^d are constants to be determined from experiments. In dimensional form, the velocity and temperature spectra become

$$E_i(K_1) = A_i^d \frac{u_*^2}{z} K_1^{-2}$$

$$E_3(K_1) = A_3^d w_*^2 K_1^{-1} \quad (10)$$

$$E_T(K_1) = B_T^d \left(\frac{g z}{T}\right)^{-2/3} \langle u'_3 T' \rangle^{\frac{4}{3}} K_1^{-1}$$

where i = 1 and 2.

The validity of these scaling laws under different stability conditions will be investigated using measurements of velocity and temperature. The measurements will also be used to estimate the similarity constants A_i, A_i^c, A_i^d, B_T, B_T^c and B_T^d.

3. Experimental Setup

An experiment was carried out from June 20 to July 2, 1993, over a dry lake bed (Owens Lake) in Owens Valley, California. The lake bed is contained in a large basin in the east of the Sierra Nevada range and west of the White and Inyo Mountains. The site is located on the northeast end of the lake bed (elevation = 1100 m). The site's surface is a heaved smooth sandy soil extending uniformly 11 km in the north-south direction and at least 4 km in the east-west direction.

The three velocity components were measured using a triaxial ultrasonic anemometer (Gill Instruments/1012R2). Sonic anemometers achieve their frequency response by sensing the effect of wind on the transit times of sound pulses traveling in opposite directions across a known path distance d_{sl}(= 0.149 m in this study). The sonic anemometer is well suited for these experiments since it is relatively free of calibration nonlinearities, atmospheric contamination drift and time lag. As shown by *Wyngaard* [1981], the main disadvantage of sonic anemometers is the wavenumber distortion due to averaging along the finite sonic path. However, this distortion is restricted to wavenumbers in excess of $2\pi/d_{sl}$ (= 42.2 m^{-1}) [see *Wyngaard*, 1981]. This limit was challenged by *Mestayer* [1982] who performed a comparison between a hot-film constant temperature anemometer and a triaxial sonic anemometer in a wind tunnel. He noted that sonic anemometer spectral distortion appears at wavenumbers 3 times smaller than that suggested by *Wyngaard* [1981]. Another comparison, which appears not to confirm *Wyngaard* [1981] spectral distortion criteria, at least on the average, was performed by *Busch* [1973] in the ASL. He compared X probe measured velocity spectra to sonic anemometer velocity spectra [*Kaimal et al.*, 1972] collected during the Kansas experiments. He noted that the local isotropy was captured by the X probe at much higher wavenumbers than that reported by *Kaimal et al.* [1972] using the sonic anemometers. However, this discrepancy may be attributed to the fact that *Kaimal et al.* [1972] combined spectra from three different heights, while *Busch*'s [1973] data were collected at 5.66 m only. For the present study we restrict our statistical analysis to a maximum wavenumber of 20 m^{-1}, but we display the full measured spectral range. The triaxial sonic anemometer sampling frequency (f_{3d}) was 56 Hz and the sampling period was 15 min. This yielded 50,400 measurements per velocity component. The absolute temperature (T) was measured from fluctuations in the measured speed of sound (c) using

$$T = \frac{c^2}{\alpha R_d} \quad (11)$$

where $\alpha = C_p/C_v$, C_p and C_v are the specific heat capacities of dry air under constant pressure and volume, respectively, and R_d is the gas constant for dry air [see *Suomi and Businger*, 1959; *Wyngaard*, 1981; *Katul*, 1994]. The influence of humidity variation on the speed of sound calculations was neglected since the maximum relative humidity (RH) recorded during the experiment was 13%. A comparison between the temperature from the triaxial sonic anemometer and the temperature fluctuation measurements from a fine wire chromel constantan thermocouple (0.0127 mm) is shown in Figure 1a. In Figure 1a the thermocouple was placed at the same height as the sonic anemometer (z = 2.5 m) but 60 cm away. The sampling frequency used in this comparison was 10 Hz. The main temperature structures are captured well by both instruments. The standard deviations of the thermocouple and sonic anemometer temperature measurements were nearly identical (0.84 °C and 0.82 °C, respectively). In Figure 1b a comparison between the power spectra of the two temperature signals is shown. The sonic anemometer temperature spectrum is shifted by two decades along the ordinate axis to permit comparison at high frequencies. At the low wavenumber end of the spectrum, the two sensors are in excellent agreement. The temperature spectrum from the thermocouple appears to "level off" at high wavenumbers due to the limited resolution of the thermocouple. The temperature spectrum of the sonic anemometer did not exhibit this phenomenon. Therefore from Figures 1a and 1b, we conclude that the sonic anemometer temperature measurements are reliable and can be used to investigate the spectral properties of turbulence. Further details about this comparison can be found in the work of *Katul et al.* [1994].

During the experiment the sonic anemometer was placed at various heights above the ground (z ranging from 2.0 m to 3.5 m above the ground). Some discussion regarding the adequacy of sonic anemometers to resolve the wavenumbers in the inertial subrange close to the ground surface is presented by *Monin and Yaglom* [1975, p. 457]. They suggested that the dimensionless frequency $f_{3d}\, z/\langle U \rangle$ should exceed 10 in order to capture the inertial subrange in the power spectrum. During this experiment the minimum height (z) and the maximum $\langle U \rangle$ were 2.0 m and 6.5 m s^{-1}, respectively, so that the minimum possible value of $f_{3d}\, z/\langle U \rangle$ = 17. Hence if an inertial subrange exists, the sonic anemometer should be capable of resolving its associated wavenumbers at these heights and sampling frequency.

The momentum roughness length z_o for the lake bed was determined from simultaneous measurements of u_* and $\langle U \rangle$ under near-neutral conditions (defined as $|z/L| < 0.1$) using

$$\langle U \rangle = \frac{u_*}{k} \ln\left(\frac{z}{z_o}\right) \quad (12)$$

Six 15-min. individual runs (not shown here), with $|z/L| < 0.1$, resulted in a mean z_o = 0.137 mm ($\pm$ 0.07 mm). The

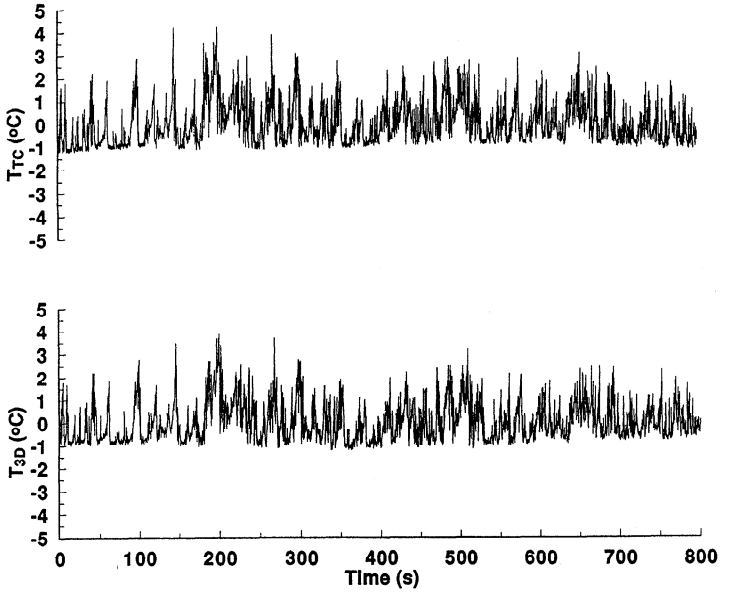

Figure 1a. A comparison between the thermocouple (T_{TC}) and the triaxial sonic anemometer (T_{3D}) temperature measurements (z = 2.5 m). The thermocouple is situated 80 cm west of the triaxial sonic anemometer. The sampling frequency is 10 Hz.

magnitude of z_o is very small so a clear distinction between smooth and rough boundary layer development may not be apparent. As shown by *Brutsaert* [1982, p. 122] and *Schlichting* [1955, p. 620], a distinction between "rough" or "smooth" boundary layer development may be based on the magnitude of the roughness Reynolds number z_{o+} (= $u_* z_o/\nu$). For rough surfaces, $z_{o+} > 2$, while for smooth surfaces, $z_{o+} < 0.13$. These criteria are adopted for classifying the roughness characteristics of the boundary layer. Differences and similarities between the statistical description of rough wall and smooth wall boundary layers is reviewed by *Raupach et al.* [1991] and *Krogstad et al.* [1992]. In a rough-wall boundary layer flow the momentum roughness length is independent of z_{o+}, whereas for a smooth boundary layer flow the dependence of z_o on z_{o+} is practically linear (see also *Schlichting* [1955], p. 122). In the transition the dependence of z_o on z_{o+} is not well understood and appears to be nonlinear.

In this study, we focus on eight 15-min. runs representing a wide range of atmospheric stability conditions. Table 1 summarizes the height, mean meteorological conditions, roughness Reynolds number, turbulent intensity and the stability parameter for all eight runs. The roughness Reynolds number values in Table 1 appear to fall within a transition region (0.13, 2) where the flow is not fully rough or smooth. The fact that desert-like surfaces are not fully rough has important consequences on extrapolating findings from agricultural or forested surfaces to deserts.

Notice from Table 1 that except for runs 1 and 3, the turbulent intensity (σ_i) in each experiment was less than 0.5 so that *Taylor*'s [1938] hypothesis can be used to convert time to space measurements (see details by *Lumley* [1965], *Powell and Elderkin* [1974], *Stull* [1988], and *Wyngaard and Clifford* [1977]). It is desirable to assess the effect of the 15-min. sampling period on the accuracy of the second moment statistics. Recall that in ASL experiments, the

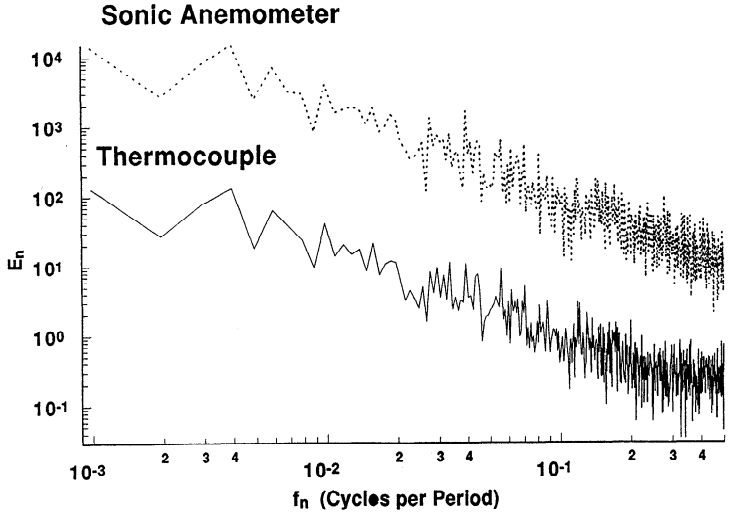

Figure 1b. A comparison between the thermocouple and the triaxial sonic anemometer temperature power spectra. To permit comparison, the triaxial sonic anemometer power spectrum is shifted by two decades relative to the thermocouple power spectrum.

Table 1. Summary of Meteorological and Stability Conditions During the Experiment

Run	Day/Time (PDST)	z (m)	L (m)	σ_1	u_*, m s^{-1}	U_1, m s^{-1}	T_a, °C	z_{o+}
1*	173/17:05	2.5	-0.64	0.71	0.11	2.17	41.2	1.0
2*	179/15:24	2.0	-3.3	0.46	0.22	5.04	44.5	2.1
3*	179/16:20	2.75	-3.1	0.64	0.19	2.0	44.3	1.8
4	179/17:10	3.5	-2.8	0.3	0.18	6.16	43.7	1.6
5	179/21:34	2.0	44.2	0.1	0.26	6.50	31.5	2.4
6	179/21:55	2.75	26.9	0.1	0.26	6.62	32.1	2.4
7	180/07:23	2.75	-46.7	0.1	0.19	4.35	25.1	1.8
8	180/07:42	2.25	-12.9	0.1	0.18	4.09	26.3	1.7

The Obukhov length L, the longitudinal velocity turbulent intensity σ_1 ($= \langle u_1'^2 \rangle^{1/2} / \langle U_1 \rangle$), the friction velocity u_*, the mean air temperature T_a at height z and the roughness Reynolds number z_{o+} are also shown. The runs for which the longitudinal velocity time series was detrended are designated by an asterisk.

Ergodic hypothesis is used to estimate the ensemble average from time averages [see *Lumley* 1970]. Because of the steady state approximation the averaging interval in many ASL experiments is finite and relatively short so that a significant error may be introduced by approximating ensemble averages with time averages, especially along the longitudinal direction (the largest integral time scales occur along this direction). As shown by *Lumley and Panofsky* [1964, p. 37], and *Wyngaard* [1992], the accuracy (e_r) due to the finite sampling period (P_T) can be estimated using

$$e_r = \left(\frac{2I_t \langle f'^2 \rangle}{\langle f^2 \rangle P_T} \right)^{\frac{1}{2}} \quad (13)$$

where I_t is the integral time scale and f is any turbulent flow variable. We note that the above formulation is derived for a Gaussian-distributed variables. Hence e_r is only an approximation of the true error since the velocity and temperature for unstable conditions are non-Gaussian. In Table 2, e_r for the longitudinal velocity is presented for all runs. The I_t values were computed from the area under the auto-correlation function of each time series up to the first zero crossing [*Sirivat and Warhaft*, 1983]. For the 15-min. averaging period, the percent error in the longitudinal velocity variance for run 1 was rather large (~23 %). For all other cases the error was acceptable. In a desert climate the mean meteorological conditions vary rapidly so that a long averaging period may violate steady state assumptions. The 15-min. sampling period was selected to be short enough to insure some steadiness in the mean meteorological conditions, while being long enough to insure adequate convergence of statistical quantities. Hence the runs are based on 15-min. averaging periods and are discussed below.

4. Results and Discussion

The power spectra E_1, E_3 and E_T were each computed from 50,400 points by consecutively windowing 16,384 points, cosine tapering 818 points along each window edge, computing the power spectrum within each window and averaging the three windowed power spectra, as discussed by *Shumway* [1988, pp. 68-73] and *Press et al.* [1990]. The dimensionless power spectra $E^{(n)}$ for near-neutral conditions are shown in Figures 2a, 2b and 2c, for moderately unstable conditions in Figures 3a, 3b and 3c, and for near-convective conditions in Figures 4a, 4b and 4c. Before considering the effect of buoyancy on the small-wavenumber turbulence

Table 2. Error Percentage Due to the Finite Averaging Period (P_t= 15 min)

Run	Day/Time	e_r(%)
1	173/1705	23.4
2	179/1524	13.8
3	179/1620	20.8
4	179/1710	6.9
5	179/2134	1.3
6	179/2155	0.7
7	180/0723	2.3
8	180/0742	1.9

Acceptable error level varies from 10 to 20% in many ASL field experiments (see Lumley and Panofsky, 1964; p. 39).

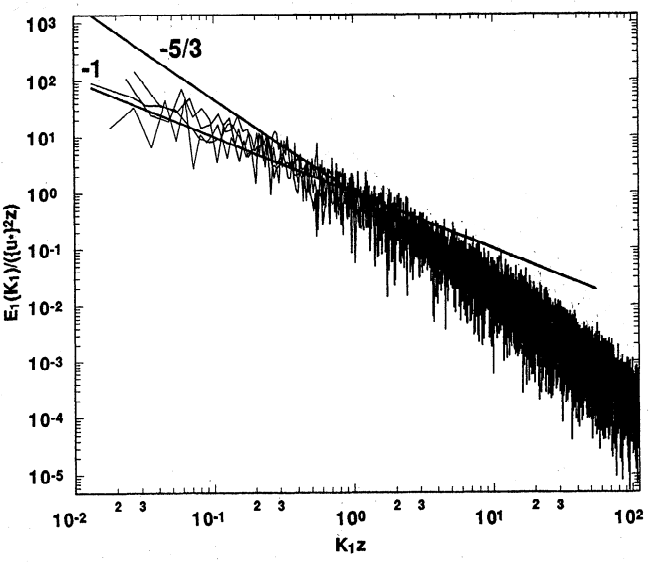

Figure 2a. Normalized longitudinal (E_1) power spectra for neutral stability conditions for runs 5, 6, 7, and 8. Taylor's hypothesis was used to convert time increments to wavenumber increments. The solid lines indicate the -5/3 and the -1 power laws.

spectra, we first consider the near-neutral atmospheric stability case.

4.1. Forced Convective Sublayer (Figures 2a, 2b and 2c)

A near-neutral ASL was assumed for runs 5-8 (see Table 1) for which $z << |L|$. This case corresponds to the dynamic sublayer for which the important parameters are u_*, z and T_*. In Figure 2a, the occurrence of a -1 power law in the longitudinal velocity was observed over one decade followed by a -5/3 power law. The vertical velocity also exhibited a limited -1 power law (see Figure 2b). Figure 2c indicates the existence of a -1 power law at low wavenumbers over one decade for the temperature measurements, which agrees with the *Metais* [1991] LES simulations. Also, notice the similarity between the temperature spectrum and the longitudinal velocity spectrum. This similarity is due to the passive role of temperature in the dynamic sublayer.

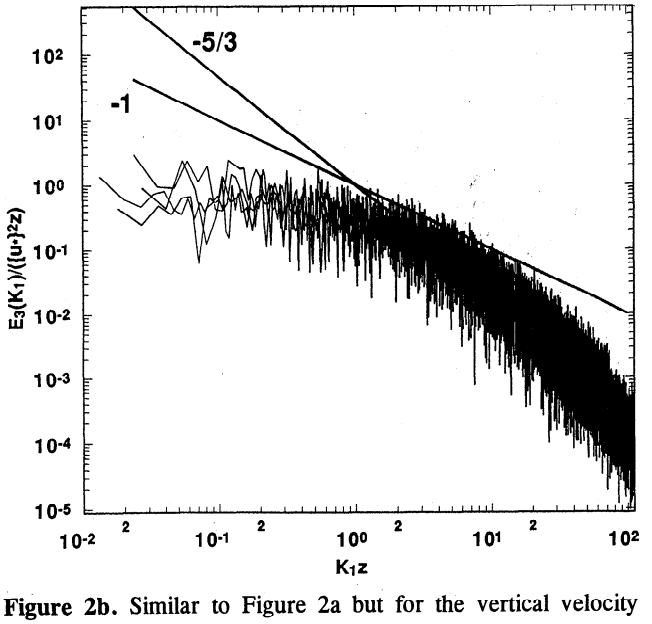

Figure 2b. Similar to Figure 2a but for the vertical velocity spectrum.

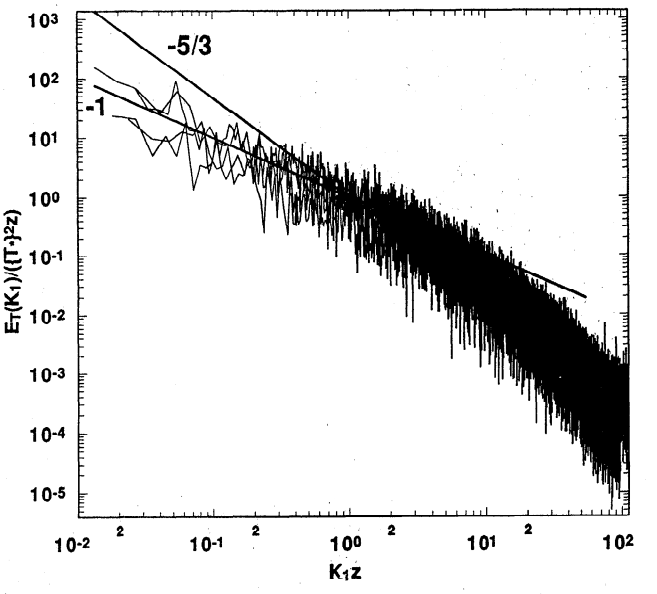

Figure 2c. Similar to Figure 2a but for the temperature spectrum.

We note that the similarity between temperature and velocity spectra in the inertial subrange was well established after the pioneering work of *Tsvang* [1960]. *Tsvang* [1960] used low-inertia resistance thermometers and a spectral analyzer to obtain the temperature spectra in the ASL. These data and many others [see *Monin and Yaglom*, 1975, pp. 494-508, for an extensive review] suggest that the local structure of temperature and velocity are similar within the inertial subrange. They did not report spectral similarity at the low-wavenumber end. Experiments by *Kaimal et al.* [1972] clearly demonstrated the effects of stability on the low-wavenumber end of the velocity spectrum but supported the hypothesized independence of the inertial subrange from $|z/L|$. Interestingly, the *Metais* [1991] LES results for an isotropic decaying turbulence advecting a passive temperature scalar revealed a -1 power law in the temperature but not in the turbulent kinetic energy.

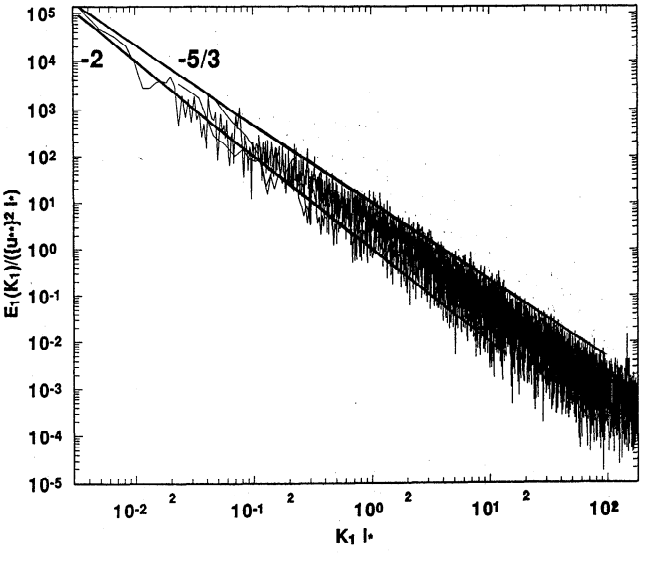

Figure 3a. Normalized longitudinal (E_1) power spectra in the dynamic convective sublayer for runs 2, 3, and 4. Taylor's hypothesis was used to convert time increments to wavenumber increments. The solid lines indicate the predicted power laws.

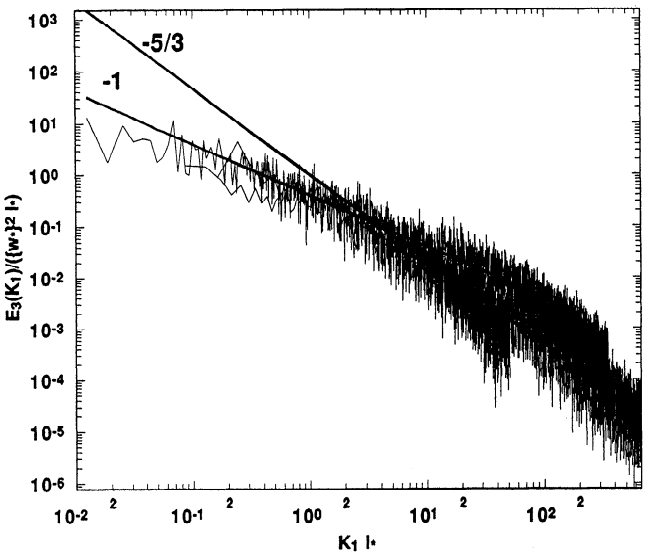

Figure 3b. Similar to Figure 3a but for the vertical velocity spectrum.

To validate the -1 power law occurrence and to determine the similarity constants (A_i and B_T), we consider the linear regression model $\text{Log}(E^{(n)}) = C_1 \text{Log}(K_1 z) + C_2$. The intercept C_2 for the spectra of horizontal, vertical velocity and temperature were used to determine the similarity constants A_1, A_3 and B_T, respectively. The results from the linear regression analysis are summarized in Table 3. The mean values of $A_1 = 1.1$, $A_3 = 0.34$ and $B_T = 0.85$ appear to agree with $A_1 = 0.95$, $A_3 = 0.35$ and $B_T = 0.9$ reported by *Káder and Yaglom* [1991] for the Tsimlyansk Field Station data (see Table 4). Also, we note that *Perry et al.* [1987] obtained a value for $A_1 = 0.90$ in their laboratory rough-wall boundary layer.

The transition from the -1 power law to the -5/3 power law appears to occur over a small range of wavenumbers. This permits an order of magnitude estimate of the wavenumbers (K_c) at which the -1 power terminates and the -5/3 power law commences. By matching the -5/3 Kolmogorov spectrum and the -1 power law spectrum at K_c, we obtain

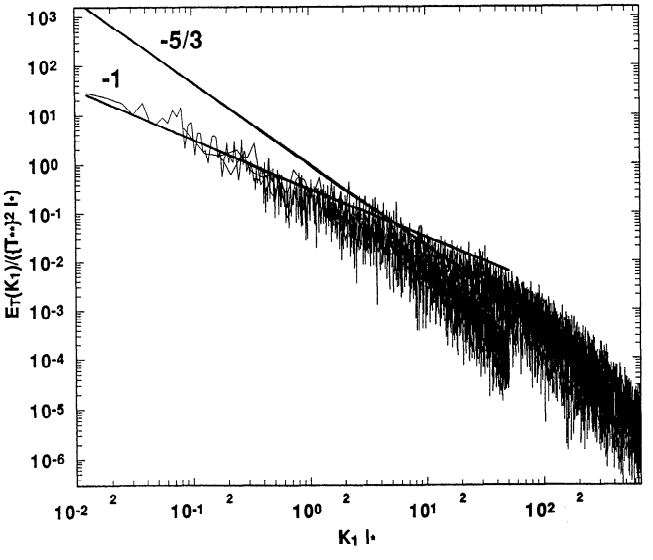

Figure 3c. Similar to Figure 3a but for the temperature power spectrum.

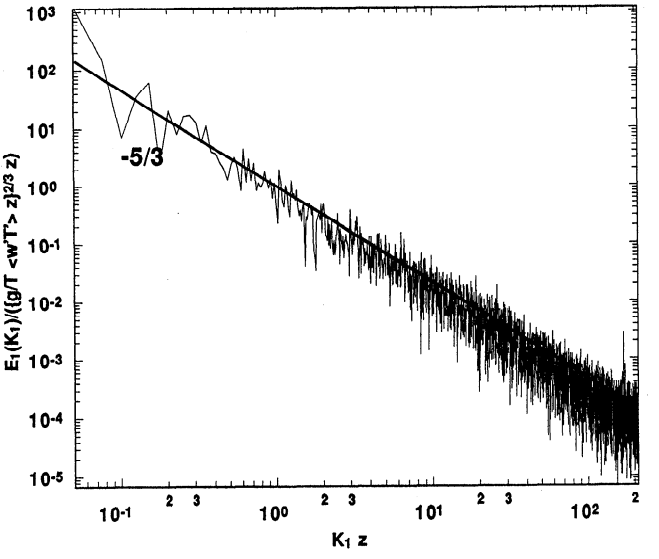

Figure 4a. Normalized longitudinal (E_1) power spectra for free convective stability conditions for run 1. Taylor's hypothesis was used to convert time increments to wavenumber increments. The solid lines indicate the predicted power laws.

$$K_c = \left(\frac{C_k}{A_1}\right)^{3/2} \frac{\langle \epsilon \rangle}{u_*^3} \tag{14}$$

where $\langle \epsilon \rangle$ is the mean turbulent kinetic energy dissipation rate and C_K is the Kolmogorov constant (= 0.55) (see *Kaimal and Finnigan* [1994], pp. 63-64). Here the internal intermittency correction to the -5/3 power law [e.g. *Kolmogorov*, 1962; *Frisch et al.*, 1978] is neglected. In the classical statistical theory of atmospheric surface layer turbulence, one assumes that energy is extracted from the mean motion and it cascades down through an inertial subrange until it is dissipated by the action of viscosity. Therefore a local conservation of energy requires that the mechanical production (for neutral ASL) is identical to the dissipation rate so that

$$\langle \epsilon \rangle = \frac{u_*^3}{kz} \tag{15}$$

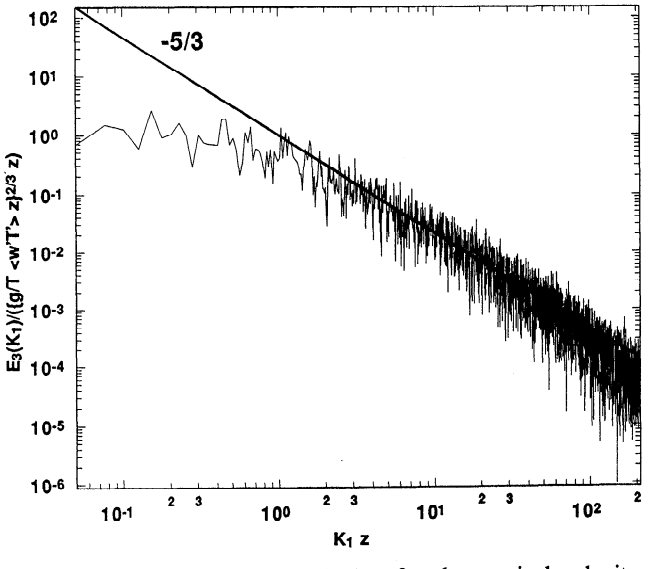

Figure 4b. Similar to Figure 4a but for the vertical velocity spectrum.

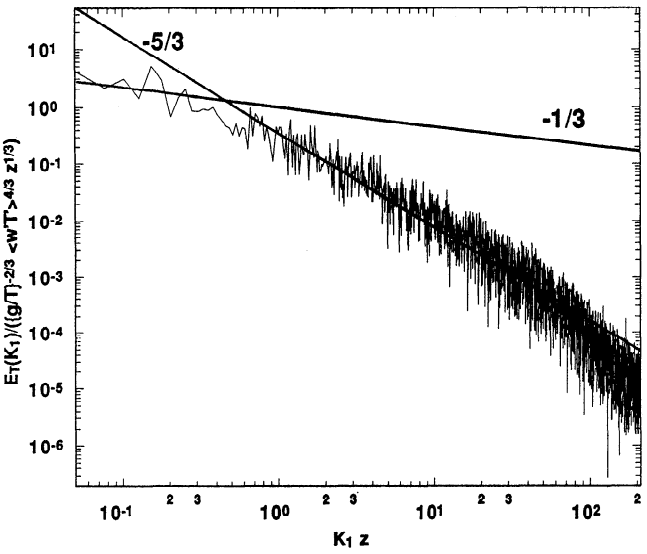

Figure 4c. Similar to Figure 4a but for the temperature spectrum.

By substituting $(u_*^3/\kappa z)$ for the mean dissipation rate, (14) reduces to

$$K_c z = \left(\frac{C_k}{A_1}\right)^{3/2}\left(\frac{1}{k}\right) \quad (16)$$

which is a constant independent of stability. For $A_1 = 1.1$, $K_c z = 0.88$, which is close to the value reported by Kader and Yaglom ($K_c z = 1.0$). The measured transition from the -1 to the -5/3 power-laws appears to vary between 0.26 and 1.1 for the longitudinal velocity, as shown in Table 3. It should be noted from Table 1 that the flow regime for runs 5 and 6 is fully rough ($z_{o+} > 2$), while for runs 7 and 8 the flow regime is not ($0.13 < z_{o+} < 2$). This may be the reason why the transition between the -1 and the -5/3 power laws are different for runs 7 and 8 ($K_c z = 0.26$) from the prediction of (16). The distinction between rough-wall and smooth-wall boundary layer flows may be important when comparing similarity constants and transitions from various studies. As shown by *Perry et al.* [1987], the constants and transitions between scaling arguments from wall-similarity theory, as extended to variances, may differ between rough-wall and smooth-wall boundary layer flows (even though the authors partially attributed these differences to instrumentation errors). In our case, one may interpret the longer -1 power law for the rough-flow case as being the result of wider range of eddy size contributing to the mechanical production.

The measured vertical velocity transition from the -1 to the -5/3 ($K_c z = 8$) is in agreement with that reported by Kader and Yaglom ($K_c z = 6.3$). The temperature power spectra exhibited a transition ($K_c z = 1.35$) from the -1 to the -5/3 power law and is also consistent with that reported by Kader and Yaglom ($K_c z = 1.4$). However, for runs 7 and 8 ($z_{o+} < 2$) this transition occurred at slightly higher wavenumbers ($K_c z = 4$).

4.2. Dynamic Convective Sublayer (Figures 3a, 3b and 3c)

Kader and Yaglom [1991] assumed that directional dimensional analysis is appropriate for $0.14 < z/|L| <$

Table 3. Scaling Parameters of Normalized Velocity and Temperature Spectra $E^{(n)}$ at Low Dimensionless Wavenumbers $K_1 z$

		$K_1 l_*$ or $K_1 z$					
Run	**Variable**	**Range**	**n**	**Slope**	**SEE**	**Constant**	**r^2**
1	U	0.05 - 7.00	278	-1.74	0.27	0.77	0.87
1	W	0.09 - 2.00	44	-1.61	0.26	0.56	0.30
1	T	0.05 - 0.26	30	-0.41	0.21	0.78	0.30
2	U	0.09 - 0.90	20	-2.04	0.20	0.09	0.90
2	W	1.00 - 35.0	379	-1.00	0.29	0.38	0.51
2	T	0.09 - 1.85	42	-1.06	0.27	0.23	0.65
3	U	0.16 - 1.70	20	-2.00	0.39	0.18	0.70
3	W	0.16 - 1.70	20	-1.00	0.26	0.35	0.58
3	T	0.16 - 2.03	24	-1.08	0.25	0.28	0.65
4	U	0.01 - 0.19	28	-2.03	0.29	0.86	0.83
4	W	0.10 - 1.00	11	-1.03	0.22	0.35	0.47
4	T	0.01 - 0.18	27	-1.09	0.23	0.32	0.69
5	U	0.01 - 1.10	164	-1.00	0.12	1.20	0.92
5	W	1.01 - 8.00	802	-1.00	0.26	0.39	0.44
5	T	0.01 - 1.20	181	-1.03	0.26	1.14	0.71
6	U	0.02 - 1.10	123	-1.00	0.29	1.10	0.66
6	W	1.08 - 10.0	1009	-1.07	0.28	0.44	0.50
6	T	0.02 - 1.50	336	-1.01	0.26	0.54	0.71
7	U	0.03 - 0.26	20	-1.08	0.30	1.03	0.45
7	W	0.80 - 8.00	534	-1.09	0.26	0.27	0.50
7	T	0.07 - 3.70	267	-1.10	0.28	0.88	0.68
8	U	0.02 - 0.26	20	-1.09	0.30	1.04	0.45
8	W	0.80 - 8.00	612	-1.08	0.26	0.27	0.50
8	T	0.02 - 4.40	373	-1.10	0.28	0.85	0.72

A regression model of the form $\log [E^{(n)}] = C_1 \text{ Log } [K_1 l_* \text{ or } K_1 z] + C_2$ is used to determine the scaling exponent. The number of points used in the regression (n), the range of dimensionless wavenumbers, the dimensionless standard error of estimate (SEE), and the coefficient of determination r^2 are also presented.

Table 4. Comparison of Computed Constants and Values Reported by Kader and Yaglom (1991) (K-Y) Are Also Shown

Stability Regime	Variable	Mean	K-Y	Variable	Range of K_z or K_l	K-Y
Forced-Convective	A_1	1.10	0.95	U	0.26-1.1	1
	A_3	0.34	0.35	W	8-10	6.3
	B_T	0.85	0.90	T	1.2-4.4	1.4
Pure-Convective	A_1^c	0.77	0.27	U	7	2
	A_3^c	0.56	0.34	W	2	3.5
	B_T	0.78	0.85	T	0.26	0.4
Dynamic-Convective	A_1^d	0.38	0.27	U	0.19-1.7	0.6
	A_3^d	0.36	0.62	W	1-35	1-10
	B_T	0.28	0.32	T	0.18-1.85	0.32

The computed constants are averaged from various Runs. The measured dimensionless transition limits from production to inertial subrange is also shown.

1.3, while the free convective dimensional similarity theory applies to $z/|L|$, > 2. These stability limits are adjusted to include von Karman constant in the definition of $|L|$. *Zilitinkevich* [1973] presented some data that appears to agree with the stability limits reported by *Kader and Yaglom* [1991]. Figures 3a, 3b and 3c present the measured dimensionless power spectra of velocity and temperature, respectively, as well as DDA slope predictions for runs 2, 3 and 4. It appears that a -2 power law scaling exists at the low-wavenumber end of the longitudinal velocity spectrum (Figure 3a) for about one decade and an extended -1 power law scaling for the vertical velocity spectrum (Figure 3b).

To determine the slopes and the constants, we consider the regression model $\text{Log}(E^{(n)}) = C_1 \text{Log}(K_l l_*) + C_2$. For the vertical velocity (Figure 3b) our data did show a surprisingly long -1 power law at the low wavenumber end of the spectrum, a range not well captured by *Kader and Yaglom*'s [1991] data. From the regression results (Table 3), the coefficient $A_3^d = 0.37$ is smaller than the value $A_3^d (= 0.62)$ reported by *Kader and Yaglom* [1991]; however, the two coefficients are comparable in magnitude. From the temperature spectrum (Figure 3b) we determined $B_T^d = 0.28$, which agrees with $B_T^d = 0.32$ reported by *Kader and Yaglom* [1991]. Table 4 summarizes the coefficients obtained from this experiment and those reported by *Kader and Yaglom* [1991].

4.3. Free Convective Sublayer (Figures 4a, 4b and 4c)

We restrict the analysis of the free convective scaling to one run only (run 1) due to the following: 1. difficulty in decomposing the time series without any ambiguity into a mean and a fluctuating part; 2. large integral time scales that prohibit the use of time averages to approximate ensemble averages; 3. difficulty in identifying runs with turbulent intensities not exceeding unity. Typically, the free convective runs are characterized by large root-mean-square velocities but low mean horizontal wind speeds. For these turbulence conditions, distortions at the low-wavenumber end due to Taylor's hypothesis can be significant. Even for run 1 the turbulent intensity is large and the results for this sublayer should be treated with caution.

Figures 4a, 4b and 4c display the normalized spectra for the longitudinal and vertical velocity, and temperature, respectively. We note that z_{o+} for this run is 1.0 and the flow regime is not fully rough. The estimated coefficients $A_1^c (= 0.77)$, $A_3^c (= 0.56)$ are higher than the values reported by *Kader and Yaglom* [1991] ($A_1^c (= 0.27)$, $A_3^c (= 0.34)$). However, the temperature coefficient $B_T^c (= 0.78)$ appears to be in better agreement with their data ($B_T^c = 0.85$). In our study (and the study by Kader and Yaglom) the range over which the -1/3 power law existed in the temperature spectrum was very narrow to permit an accurate estimate of B_T^c. We also note that the limits at which the free convective scaling terminates and the inertial subrange initiates are in close agreement with the limits reported by Kader and Yaglom (see Table 3) for temperature. For the velocity, this was not the case since a -5/3 power law exists for both inertial and production regimes.

5. Conclusions

This study has focused on the low-wavenumber spectral characteristics of velocity and temperature in the atmospheric surface layer under different stability conditions. Velocity and temperature were measured using a triaxial sonic anemometer over a dry lake bed. The momentum roughness length of the lake bed was very small ($z_o = 0.13$ mm) and the flow regime was not clearly bluff rough.

Under near-neutral conditions both temperature and velocity spectra exhibited a -1 power law followed by a -5/3 power law, which was consistent with other laboratory and field studies of boundary layer flows. The -1 power law was derived using the dimensional analysis method proposed by *Perry et al.* [1977] and *Kader and Yaglom* [1991]. A key assumption in this analysis was the height independence of the power spectrum at the low-wavenumber end for small heights. The similarity coefficients obtained from the measured velocity and temperature spectra were in good agreement with earlier values reported by *Kader and Yaglom*

[1991] and *Perry et al.* [1987]. We assumed that the transition between the -1 power law and the inertial subrange was very narrow so that matching the inertial subrange power law to the -1 power law at one wavenumber is reasonable. This transition wavenumber was derived as a function of the Kolmogorov and von Karman constants and agreed well with the measured transition wavenumber for the fully rough flow conditions. When the roughness Reynolds number was small, the transition occurred at lower wavenumbers. This indicated that for fully rough flow conditions a wider range of eddy sizes were responsible for the mechanical production of turbulence.

For moderately unstable conditions, directional dimensional analysis was used to predict the power law exponents for the velocity and temperature spectra. A key assumption in this analysis was the independence of the mechanical and buoyant production of turbulence. This independence permitted the definition of two length scales that were used to scale horizontal and vertical statistics. It was demonstrated that the vertical velocity and temperature power spectra still exhibited a -1 power law; however, the longitudinal velocity power spectrum followed a -2 power law. The proportionality constants derived from our experiment partially agree with previously reported values. Also, the transition from production wavenumbers to inertial subrange wavenumbers was consistent with *Kader and Yaglom* [1991] data.

We analyzed the velocity and temperature spectra for free convective conditions. Because of unsteadiness in the mean meteorological condition and large turbulent intensity, only one run was selected for analysis. For the velocity time series of this run, a -5/3 power law was derived for both production and inertial subrange wavenumbers. The distinction between the two regimes was not very apparent. The temperature power spectrum did exhibit a -1/3 power law for less than a decade of wavenumbers in agreement with free convective scaling and Kader and Yaglom's data.

Acknowledgments. The authors would like to thank Scott Tyler for his assistance and support at Owens Lake, Sergej Zilitinkevich for pointing out his 1973 paper, passing along his recent manuscript and providing very helpful comments, and Mike Mata for his help in the data collection. We are grateful for the funding support from the National Science Foundation (NSF) grant (EAR-93-04331), U.S. Geological Survey (USGS), Water Resources Center (WRC) grant (W-812), Kearney Foundation and UC Davis superfund grant (5P42ES04699-07).

References

Antonia, R.A., and MR. Raupach, Spectral scaling laws in a high Reynolds number laboratory boundary layer, *Boundary Layer Meteor.*, *65*, 289-306, 1993.

Betchov, R., and A.M. Yaglom, Comments on the theory of similarity as applied to turbulence in an unstable stratified fluid, *Izv. Akad. Nauk. Ser. Fiz. Atmos. Okeana, Eng. Trans.*, *7*, 829-832, 1971.

Brutsaert, W., *Evaporation into the Atmosphere: Theory, History, and Applications*, 299 pp., *Kluwer Academic*, Norwell, Mass., 1982

Busch, N.E., The surface boundary layer, *Boundary Layer Meteorol.*, *4*, 213-240, 1973.

Erm, L.P., and P.N. Joubert, Low Reynolds number turbulent boundary layers, *J. Fluid Mech.*, *230*, 1-44, 1991.

Frisch, U., P.L. Sulem, and M. Nelkin, A simple dynamical model of intermittent fully developed turbulence, *J. Fluid Mech.*, *87*, 719-36, 1978.

Garratt, J.R., *The Atmospheric Boundary Layer*, 316 pp., *Cambridge University Press*, New York, 1992.

Hinze, J.O., *Turbulence*, 790 pp., *McGraw-Hill*, New York, 1959.

Kader, B.A., and A.M. Yaglom, Turbulent structure of an unstable atmospheric layer, *Nonlinear and Turbulent Processes in Physics*, edited by R.Z. Sagdeyev, vol. 2, pp. 829-845, *Harwood Academic*, Boston, Mass, 1984.

Kader, B.A., and A.M. Yaglom, Mean fields and fluctuation moments in unstably stratified turbulent boundary layer, *J. Fluid Mech.*, *212*, 637-662, 1990.

Kader, B.A., and A.M. Yaglom, Spectra and correlation functions of surface layer atmospoheric turbulence in unstable thermal stratification, *Turbulence and Coherent Structures*,. edited by O. Metais and M. Lesieur, 450 pp., *Kluwer Academic*, Norwell, Mass., 1991.

Kaimal, J.C., and J.J. Finnigan, *Atmospheric Boundary Layer Flows: Their Structure and Measurement*, 289 pp., *Oxford University Press*, 1994

Kaimal, J.C., J.C. Wyngaard, Y. Izumi, and O.R. Cote. Spectral characteristics of surface layer turbulence, *J. R. Meterol. Soc.*, *98*, 563-589, 1972.

Katul, G., A model for sensible heat flux probability density function for near-neutral and slightly-stable atmospheric flows, *Boundary Layer Meteor.*, *71*, 1-20 1994.

Katul, G., M. Parlange, and C.R. Chu, Intermittency, local isotropy, and non-Gaussian statistics in stratified atmospheric surface layer turbulent flows, *Phys. Fluids*, *6*, pp. 2480-2492, 1994.

Klebanoff, P.S. Characteristics of turbulence in a boundary layer with zero-pressure gradient, *Rep. 1247*, pp. 1-28, *Natl. Advisory Comm. for Aeronaut.*, 1954.

Kolmogorov, A.N. The local structure of turbulence in incompressible viscous fluid for very large Reynolds numbers, *Dokl. Akad. Nauk SSSR*, *4*, 299-303, 1941.

Kolmogorov, A.N., A refinement of previous hypothesis concerning the local structure of turbulence in a viscous incompressible fluid at high Reynolds number, *J. Fluid Mech.*, *13*, 82-85, 1962.

Korotkov, B.N., Some types of local self-similarity of the velocity field of wall turbulent flows, *Izv. Akad. Nauk. Ser. Mekh. Zhidk. i. Gaza*, *6*, 35-42, 1976.

Krogstad, P.A., R.A. Antonia, and W.B. Browne. Comparison between rough and smooth wall turbulent boundary layers, *J. Fluid Mech.*, *245*, 599-617, 1992.

Lesieur, M., and R. Rogallo. Large eddy simulation of passive scalar diffusion in isotropic turbulence, *Phys. Fluids*, *4*, 718-722, 1989.

Lumley, J. Interpretation of time spectra measured in high intensity shear flows, *Phys. Fluids*, *6*, 1056-1062, 1965.

Lumley, J. *Stochastic Tools in Turbulence*, 194 pp., *Academic*, San Diego, Calif., 1970.

Lumley, J., and H. Panofsky *The Structure of Atmospheric Turbulence*, 239 pp., *John Wiley*, New York, 1964.

Metais, O. Large-eddy simulation of turbulent scalar: The influence of intermittency, *The Global Geometry of Turbulence*, edited by J. Jimenez, pp. 155-166, *Plenum*, New York, 1991.

Metais, O., and M. Lesieur. Spectral large eddy simulation of isotropic and stably stratified turbulence, *J. Fluid Mech.*, *239*, 157-194, 1992.

Mestayer, P. Local isotropy and anisotropy in a high-Reynolds number turbulent boundary layer, *J. Fluid Mech.*, *125*, 475-503, 1982.

Millikan, C.B. A critical discussion of turbulent flow in channels and circular tubes, in *Proceedings of the Fifth International Congress on Applied Mechanics*, pp. 386-392, John Wiley, New York, 1939

Monin, A.S., and A.M. Obukhov. Basic laws of turbulent mixing in the ground layer of the atmosphere, *Tr. Geofiz. Inst. Akad. Nauk*, *151*, 163-187, 1954.

Monin, A.S., and A.M. Yaglom. *Statistical Fluid Mechanics*, vol.I, edited by J. Lumley, 768 pp, *MIT Press*, Cambridge, Mass., 1971.

Monin, A.S., and A.M. Yaglom. *Statistical Fluid Mechanics*, vol.II, edited by J. Lumley, 874 pp., *MIT Press*, 1975.

Panton, R.L. *Incompressible Flow*, 780 pp., *Wiley-Interscience*, New York, 1984.

Peixoto, J.P., and A.H. Oort, *Physics of Climate*, 520 pp., *American Institute of Physics*, New York, 1992.

Perry, A.E., and C.J. Abell. Scaling laws for pipe flow turbulence, *J. Fluid Mech.*, *67*, 257-271, 1975.

Perry, A.E., and C.J. Abell. Asymptotic similarity of turbulence structures in smooth and rough-walled pipes, *J. Fluid Mech.*, *79*, 785-799, 1977.

Perry, A.E., and M.S. Chong. On the mechanism of wall turbulence, *J. Fluid Mech.*, *119*, 173-217, 1982.

Perry, A.E., and J.D. Li. Experimental support for the attached eddy hypothesis in zero pressure gradient turbulent boundary layer, *J. Fluid Mech.*, *218*, 405-438, 1990.

Perry, A.E., S. Henbest, and M.S. Chong. A theoretical and experimental study of wall turbulence, *J. Fluid Mech.*, *165*, 163-199, 1986.

Perry, A.E., K.L. Lim, and S.M. Henbest. An experimental study of turbulence structure in smooth and rough-wall turbulent boundary layers, *J. Fluid Mech.*, *165*, 163-199, 1987.

Perry, A.E., J.D. Li, and I. Marusic. Towards a closure scheme for turbulent boundary layers using the attached eddy hypothesis, in *Turbulent Flow Structure Near Walls*, edited by J.D.A. Walker, pp. 67-79, *London Royal Society*, 1991.

Perry, A.E., I. Marusic, and J.D. Li. Wall turbulence closure based on classical similarity laws and the attached eddy hypothesis, *Phys. Fluids*, *6*, 1024-1035, 1994.

Powell, D., and C.E. Elderkin. An investigation of the application of Taylor's hypothesis to atmospheric boundary layer turbulence, *J. Atmos. Sci.*, *31*, 990-1002, 1974.

Press, W.H., B.P. Flannery, S.A. Teukolsky, and W.T. Vetterling. *Numerical Receipes: The Art of Scientific Computing*, 702 pp., *Cambridge University Press*, New York, 1990.

Raupach, M.R., R.A. Antonia, and S. Rajagopalan. Rough-wall turbulent boundary layers, *Appl. Mech. Rev.*, *44*, 1-25, 1991.

Schlichting, H. *Boundary-Layer Theory*, 817 pp., *McGraw-Hill*, New York, 1955.

Shumway, R.H.. *Applied Statistical Time Series Analysis*, 379 pp., *Prentice-Hall*, Englewood Cliffs, N.J., 1988.

Sirivat, A., and Z. Warhaft. The effect of a passive cross-stream temperature gradient on the evolution of temperature variance and heat flux in grid turbulence, *J. Fluid Mech.*, *128*, 323-346, 1983.

Stull, R. *An Introduction to Boundary Layer Meteorology*, 666 pp., *Kluwer Academic*, Norwell, Mass.,.1988

Suomi, V.E., and J.A. Businger. Sonic anemometer-thermometer, *Geophys. Res. Pap.*, *59*, 1-60, 1959.

Taylor, G.I. The spectrum of turbulence, *Proc. Roy. Soc. A*, *CLXIV*, 476-490, 1938.

Tchen, C.M. On the spectrum of energy in turbulent shear flow, *Natl. Bur. of Stand.*, *50*, 51-62, 1953.

Tennekes, H., and J. Lumley. *A First Course in Turbulence*, 300 pp., *MIT Press*, Cambridge, Mass, 1972.

Townsend, A.A. *The Structure of Turbulent Shear Flow*, 429 pp., *Cambridge University Press*,.New York, 1976.

Tsvang, L.R. Measurements of the frequency spectra of temperature fluctuations in the surface layer of the atmosphere, *Izv. Akad. Nauk., Ser. Geofiz.*, *8*, 1252-1262, 1960.

von Karman, T. Mechanische Ahnlichkeit und Turbulenz, *Nachr. Wiss. Gottingen*, Math. Phys. Kl., 58, 1930.

Wyngaard, J.C. Cup, propeller, vane, and sonic anemometer in turbulence research, *Ann. Rev. Fluid Mech.*, *13*, 922-929, 1981.

Wyngaard, J.C. Atmospheric turbulence, *Ann. Rev. Fluid Mech.*, *24*, 205-233, 1992.

Wyngaard, J.C., and S.F. Clifford. Taylor's hypothesis and high-frequency turbulence spectra, *J. Atmos. Sci.*, *34*, 399-423, 1977.

Zilitinkevich, S.S. On the turbulence and diffusion under free convection conditions, *Izv. Akad. Nauk., Ser. Fiz. Atmos. Okeana*, *7*, 1263-1269, 1971.

Zilitinkevich, S.S. Shear convection, *Boundary Layer Meteorol.*, *3*, 416-423, 1973.

J.D. Albertson, T.A. Ortenburger and M.B. Parlange, Hydrologic Science, University of California, Davis, CA 95616.

C.R. Chu, Department of Civil Engineering, National Central University, Chung-Li, Taiwan., R.O.C.

G.G. Katul, School of the Environment, Box 90328, Duke University, Durham, NC 27708-0328.

(Received December 1, 1993; revised September 23, 1994; accepted September 23, 1994.)